

12

RADC-TR-82-295, Vol I (of two)
Interim Report
November 1982



AD A124745

ACOSS-11 (ACTIVE CONTROL OF SPACE STRUCTURES)

The Charles Stark Draper Laboratory, Inc.

Sponsored by
Defense Advanced Research Projects Agency (DOD)
ARPA Order No. 3655

APPROVED FOR PUBLIC RELEASE; DISTRIBUTION UNLIMITED

The views and conclusions contained in this document are those of the authors and should not be interpreted as necessarily representing the official policies, either expressed or implied, of the Defense Advanced Research Projects Agency or the U.S. Government.

DTIC FILE COPY

ROME AIR DEVELOPMENT CENTER
Air Force Systems Command
Griffiss Air Force Base, NY 13441

DTIC
ELECTE
FEB 23 1983
S D
E

83 02 022 065

This report has been reviewed by the RADC Public Affairs Office (PA) and is releasable to the National Technical Information Service (NTIS). At NTIS it will be releasable to the general public, including foreign nations.

RADC-TR-82-295, Volume I (of two) has been reviewed and is approved for publication.

APPROVED:



RICHARD W. CARMAN
Project Engineer

APPROVED:



FRANK J. REHM
Technical Director
Surveillance Division

FOR THE COMMANDER:



JOHN P. HUSS
Acting Chief, Plans Office

If your address has changed or if you wish to be removed from the RADC mailing list, or if the addressee is no longer employed by your organization, please notify RADC (OCSE) Griffiss AFB NY 13441. This will assist us in maintaining a current mailing list.

Do not return copies of this report unless contractual obligations or notices on a specific document requires that it be returned.

Volume I

ACOSS-11 (ACTIVE CONTROL OF SPACE STRUCTURES)

T. H. Brooks
V. N. Mahajan

Contractor: The Charles Stark Draper Laboratory, Inc.
Contract Number: F30602-81-C-0180
Effective Date of Contract: 27 April 1981
Contract Expiration Date: 27 April 1984
Short Title of Work: AcoSS-11 (Active Control of Space
Structures)
Program Code Number: 1E20
Period of Work Covered: Nov 81 - Apr 82
Principal Investigator: Dr. Keto Soosaar
Phone: 617 258-2575
Project Engineer: Richard M. Carman
Phone: 315 330-3148

Approved for public release; distribution unlimited.

This research was supported by the Defense Advanced Research Projects Agency of the Department of Defense and was monitored by Richard M. Carman (RADC/OCSE), Griffiss AFB NY 13441 under Contract F30602-81-C-0180.

UNCLASSIFIED

SECURITY CLASSIFICATION OF THIS PAGE (When Data Entered)

REPORT DOCUMENTATION PAGE		READ INSTRUCTIONS BEFORE COMPLETING FORM
1. REPORT NUMBER RADC-TR-82-295, Vol I (of two)	2. GOVT ACCESSION NO. AD-A124 743	3. RECIPIENT'S CATALOG NUMBER
4. TITLE (and Subtitle) ACOSS-11 (ACTIVE CONTROL OF SPACE STRUCTURES)		5. TYPE OF REPORT & PERIOD COVERED Interim Report Nov 81 - Apr 82
		6. PERFORMING ORG. REPORT NUMBER N/A CSDL-R-1538.-
7. AUTHOR(s) T. H. Brooks V. N. Mahajan		8. CONTRACT OR GRANT NUMBER(s) F30602-81-C-0180
9. PERFORMING ORGANIZATION NAME AND ADDRESS The Charles Stark Draper Laboratory, Inc. 555 Technology Square Cambridge MA 02139		10. PROGRAM ELEMENT, PROJECT, TASK AREA & WORK UNIT NUMBERS 62301E C6550116
11. CONTROLLING OFFICE NAME AND ADDRESS Defense Advanced Research Projects Agency 1400 Wilson Blvd Arlington VA 22209		12. REPORT DATE November 1982
		13. NUMBER OF PAGES 68
14. MONITORING AGENCY NAME & ADDRESS (if different from Controlling Office) Rome Air Development Center (OCSE) Griffiss AFB NY 13441		15. SECURITY CLASS. (of this report) UNCLASSIFIED
		15a. DECLASSIFICATION/DOWNGRADING SCHEDULE N/A
16. DISTRIBUTION STATEMENT (of this Report) Approved for public release; distribution unlimited.		
17. DISTRIBUTION STATEMENT (of the abstract entered in Block 20, if different from Report) Same		
18. SUPPLEMENTARY NOTES RADC Project Engineer: Richard M. Carman (OCSE)		
19. KEY WORDS (Continue on reverse side if necessary and identify by block number)		
Simulated Terrestrial Scenes	DMA Data	Image Sharpening
Generic Scene Simulation	Aberrations	Deconvolution
Genesis	Zernike Polynomials	Mirror Deformations
Draper Integrated Simulations	Phase Retrieval	
20. ABSTRACT (Continue on reverse side if necessary and identify by block number) <u>Simulation Extensions</u>		
In analysis and simulation of space-based surveillance system performance, a key variable is the scene/sensor integration. Under subcontract to CSDL, Photon Research Associates is developing a software package capable of generating a manipulating terrestrial scene data sets as a function of major surveillance system and mission parameters. This package, when		

DD FORM 1473
1 JAN 73

EDITION OF 1 NOV 65 IS OBSOLETE

UNCLASSIFIED

SECURITY CLASSIFICATION OF THIS PAGE (When Data Entered)

UNCLASSIFIED

SECURITY CLASSIFICATION OF THIS PAGE(When Data Entered)

incorporated into the Draper Integrated Simulations, will result in a broad and comprehensive tool for the analysis and simulation of space based surveillance system performance.

Halo Optics

CSDL prepared phase retrieval tests using cryogenic deformations of an Itek HALO mirror. It is shown that Eikonix phase retrieval algorithms did not succeed on these blind tests. CSDL's image sharpening algorithm was successful in improving image quality. It is recommended that another blind test be prepared. Moreover, plans for hardware tests should also be initiated.

Active Controller Designs

Volume 2 of this report describes progress in the application of active controller design methods to the ACROSS Model No. 2 structure. Attention is focused on attenuation of the effects of a broad-band disturbance input upon line-of-sight rotation error, and upon the generation of smooth large-angle slew maneuvers.

A

UNCLASSIFIED

SECURITY CLASSIFICATION OF THIS PAGE(When Data Entered)

ACKNOWLEDGEMENT

This report was prepared by The Charles Stark Draper Laboratory, Inc., under Contract F30602-81-C-0180. This research was supported by the Advanced Research Projects Agency of the Department of Defense and monitored by the Rome Air Development Center.

The program manager is Dr. Keto Soosaar and the project leaders are Mr. Thomas H. Brooks for Simulations Extension, Dr. Virendra N. Mahajan for HALO Optics, and Mr. Robert R. Strunce for Active Control of Space Structures (ACOSS). The authors of Volume 1 of this report are: Mr. Thomas H. Brooks (Section 2) and Dr. Virendra N. Mahajan (Section 3).

Publication of this report does not constitute approval by the Defense Advanced Research Projects Agency or the U.S. Government of the findings or conclusions contained herein. It is published for the exchange and stimulation of ideas.



Accession For	
NTIS GRA&I	<input checked="" type="checkbox"/>
DTIC TAB	<input type="checkbox"/>
Unannounced	<input type="checkbox"/>
Justification _____	
By _____	
Distribution/	
Availability Codes	
Dist	Avail and/or Special
A	

VOLUME 1

TABLE OF CONTENTS

<u>Section</u>		<u>Page</u>
1	INTRODUCTION	1-1
1.1	Simulation Extension	1-1
1.2	HALO Optics	1-2
1.3	Active Control of Space Structures (ACOSS)	1-2
1.3.1	Scope	1-2
1.3.2	Limitations	1-5
2	SIMULATION EXTENSION	2-1
2.0	Introduction	2-1
2.1	Code Architecture	2-2
2.1.1	Modules	2-3
2.2.2	Module Interaction	2-3
2.1.3	User Input/Control	2-4
2.1.4	Scene Data Base Inputs	2-6
2.2	Module Description	2-6
2.2.1	Geometry	2-6
2.2.2	Atmospheric Module	2-7
2.2.3	Heat Transfer	2-9
2.2.4	Radiance Module	2-19
2.2.5	Imaging	2-22

<u>Section</u>		<u>Page</u>
3	HALO OPTICS	3-1
3.0	Introduction	3-1
3.1	Aberration Analysis	3-1
3.2	Phase Retrieval Test Results	3-4
3.3	Image Sharpening Test Results	3-10
3.4	Summary, Conclusions, and Recommendations	3-10

SECTION 1

INTRODUCTION

1.1 Simulation Extension

In support of the Draper Integrated Simulations, Photon Research Associates (PRA) was placed under subcontract to develop a computer code capable of generating and manipulating terrestrial scenes as a function of major surveillance system and mission parameters. This code (called GENESSIS) will have the capability to interface with the DMA data base on terrestrial scenes as the source of scene input data. Consequently, the code will be able to simulate any scene for which DMA data exists. To have a functioning code as soon as possible, it is planned to develop the code in three phases, the first phase (i.e., the present subcontract) provides a functional synthetic scene computer code. When all three phases of the program are complete, GENESSIS will treat all phenomenological and functional aspects of scene simulation without recourse to simplifying approximations, and will be fully interfaced with the DMA data base. At the end of the first phase a limited capability will be provided for a limited number of scenes. During the current reporting period the code has been essentially completed, with all modules in the final stages of verification and validation. Code integration has begun and the input data bases are being accumulated. The progress and accomplishments of PRA during the first six months of their one year sub-contract are described in Section 2.

1.2 HALO Optics

CSDL supports DARPA on HALO optics technology by preparing and evaluating test cases for HALO system alignment and wavefront control. Three contractors have been working on the general problem of HALO alignment. Eikonix Corporation has worked on the phase retrieval problems, i.e., determination of system aberrations from the focal-plane image data. Itek Corporation uses a wavefront sensor to measure the system aberrations. These aberrations are decomposed into mirror figure errors which are then corrected with actuators. Hughes Aircraft has worked on the problem of optical system correction using "color" algorithms on the focal-plane data.

In our previous semi-annual report, we reported preparation of phase retrieval tests for the Eikonix phase retrieval algorithms. An update on the test results is provided in the current report. It is shown that the algorithms did not succeed on the blind test. The algorithms worked when we disclosed all the information to Eikonix. CSDL's image sharpening algorithm did succeed on the test, improving the Strehl ratio of the degraded image from 0.255 to 0.616.

1.3 Active Control of Space Structures (ACOSS)

1.3.1 Scope

Volume 2 of the present report gives an account of the progress made during the reporting period in implementing various strategies for active control on ACOSS Model No. 2. The design objective for the several vibration control strategies employed is to attenuate the line-of-sight (LOS) rotation error and defocus of the optical system induced by a broad-band disturbance. A slewing controller for implementing large changes in the rigid-body attitude of the structure with minimal associated line-of-sight error is also studied.

1.3.1.1 Vibration Control

A general form of disturbance containing both broad-band and discrete-frequency components has been communicated by Riverside Research Institute to assist in comparing competing designs of vibration controllers. Several modifications of this disturbance specification are made for the purpose of the present study in order to reduce computation costs. First, the bandwidth of the broad-band portion is 5 Hz., extending from 0 Hz. to 5 Hz. The reduction of the upper boundary from 15 Hz. to 5 Hz. is dictated by the reduced-order model (20 modes) being studied. The extension of the lower boundary to 0 Hz. enables the use of a simpler model of the disturbance without sacrifice of fidelity since rigid-body modes are not studied in the disturbance-rejection problem. Second, the disturbance is assumed to be fixed in direction at each specified point of application to the structure, varying stochastically only in magnitude. In addition, the one-sided spectral density amplitude in the specification is retained for two-sided use. Details are presented in Section 2. These modifications do not alter the qualitative objective of the study; namely, to examine the fundamental difficulties associated with designing vibration controllers to stringent LOS-error tolerances in the presence of a broad-band disturbance.

A selection of structural vibration modes to be considered in the various designs, and a corresponding selection to be used in evaluating the designs, is determined by ranking each of the 156 structural modes in the NASTRAN finite element model with respect to the root-mean-square (RMS) error in LOS-rotation that results from the disturbance acting on that mode (viewed as a single channel). The highest ranking ten modes according to this criterion are chosen to constitute the model for the control designs, and the highest ranking twenty modes constitute the evaluation model. The upper limit on the number of modes to be included is chosen with consideration of the computation cost. The modes selected and their ranking are also given in Section 2.

A choice of location for sensors and actuators for the controller design is determined using an original approach particularly suited to the stringent performance requirements in the present design problem. Locations are chosen using algebraic methods which make explicit the contributions to the LOS-error associated with particular sensors or actuators. Details are given in Section 3.

Three different approaches to the design of a vibration controller are presented. The first approach, disturbance-rejection control, assumes that complete information on the statistical properties of the disturbance is available. Using this information, a stochastic dynamic model of the disturbance is concatenated with the open-loop design model of the structure. A linear-quadratic-Gaussian (LQG) controller for the enlarged system is designed. The design process involves a few iterations in which weighting matrices are adjusted to achieve the desired performance. Details are given in Section 4. Satisfactory attenuation of the disturbance effects upon LOS-rotation error is achieved. It is important to note that this attenuation is achieved by moving the characteristic frequencies of the closed-loop system outside the bandwidth of the disturbance, as well as by adding damping to the different modes.

In the second approach, linear-quadratic (LQ) optimal control, more realistic assumptions with regard to the knowledge of the disturbance characteristics are made. The disturbance statistics are not assumed to be known. Instead, the effect of the disturbance, as reflected in the RMS values of the LOS-rotation error, is used to select desired values for closed-loop modal characteristic frequencies and damping ratios. Well-known relationships connecting closed-loop modal parameter values and weighting matrices for LQ design are exploited, thus generating a systematic analytical approach to the selection of

weighting matrices. Details are given in Section 5. As in the first design approach, results show that LOS-error reduction is obtained principally by augmentation of stiffness rather than of damping.

The third design approach is an extension of the second approach; actuator synthesizers are incorporated into the design to alleviate the problem of control spillover to certain modeled modes not in the controller design model. Details are given in Section 6.

1.3.1.2 Large-Angle Slew Control

A large-angle slew maneuver involves an input of energy to the vehicle which, in turn, induces vibration in the optical support structure. The control problem is to apply the energy to the structure in such a way that the desired attitude maneuver is accomplished and that the optical system supported by the structure returns rapidly to acceptable levels of performance following the maneuver. Several significant extensions to previous work are reported here. One is to solve the problem of slew to a moving, rather than a fixed, target. The other is the development of a closed-loop control strategy using integral compensation based on measurements which include control and control rate signals, rather than a strategy based only on open-loop considerations. Details are given in Section 7.

1.3.2 Limitations

The present report gives an account of work in progress, rather than of completed work. The quantitative results in particular should be viewed in that light.

With respect to the vibration control designs, the present report does not include an account of an evaluation of the ten-mode controller designs against the twenty-mode evaluation model, or the

effects of the use of an observer in the deterministic LQ controller designs. Investigations on these matters are in progress and will be reported on subsequently.

Substantial work has also been done in other related areas, such as suboptimal output feedback, modal-spring-plus-modal-dashpot output feedback, and system identification, in relation to ACOSS Model No 2. In addition, fundamental investigations have been launched into problems associated with the explicit incorporation of the dynamics of actuators and of data-sampling devices into the mathematical model for the structure and controller. Accounts of this work will be reported in the future.

SECTION 2

SIMULATION EXTENSION

2.0 Introduction

In support of the Draper Integrated Simulations, Photon Research Associates (PRA) was placed under subcontract to develop a computer code capable of generating and manipulating terrestrial scenes as a function of major surveillance system and mission parameters. This code (called GENESSIS) will have the capability to interface with the DMA data base on terrestrial scenes as the source of scene input data. Consequently, the code will be able to simulate any scene for which DMA data exists. Because it is desirable to have a functioning code as soon as possible, it is planned to develop the code in three phases, the first phase (i.e., the present subcontract) providing a functional synthetic scene simulation computer code. In the paragraphs to follow, the progress and accomplishments of PRA during the first six months of their one year sub-contract are described.

To achieve these goals the first-phase code will have three basic limitations. First, some of the higher-order phenomena controlling scene radiance (e.g., cloud shadowing) will be neglected. Second, some of the phenomenological treatments will utilize simplifying approximations. Last, the input data base will be limited to five terrestrial scenes and two cloud representations. It is planned to eliminate these limitations during subsequent phases. In particular, it is anticipated that the full interface with DMA data will have been accomplished by the end of the second phase.

In summary, when all three phases of the program are complete, GENESSIS will treat all phenomenological and functional aspects of scene simulation without recourse to simplifying approximations, and will be fully interfaced with the DMA data base. At the end of the first phase a limited capability will be provided for a limited number of scenes. During the current reporting period the code has been essentially completed, with all modules in the final stages of verification and validation. Code integration has begun and the input data bases are being accumulated.

2.1 Code Architecture

Scene simulation is based upon a point-by-point algorithm, a single cycle which consists of collecting (and in some instances, computing) inputs specific to a single point on the scene, calculating the apparent radiance of that point from the collected inputs, and finally weighting and assigning the calculated radiance to the appropriate pixel in the observer's field of view. If the density of points is large enough, the scene is properly sampled and the radiances computed by repeated point calculations can be combined to produce an accurate pixel radiance map of the scene. The parameters of these radiance grid points are computed from the three-dimensional scene itself.

Scene data consists of discrete altitude and material type pairs specified at regular intervals on a planar rectangular grid. Continuous surfaces are produced from the discrete scene data using a bi-cubic spline fitting technique. Point data can be computed from these surfaces at any desired spatial resolution.

The computed apparent radiance consists of four terms combined additively. These are reflected solar, thermal emission, reflected skyshine and path radiance. These respective calculational procedures are discussed in Section 2.2.4. Each major calculational operation is

performed with a separate software module. Each module has stand-alone capabilities, but are normally executed in sequence to produce a final result.

The simulations' primary output is an N X M viewer-perspective pixel apparent radiance map. Diagnostic output is also available to check on the proper running of the code.

2.1.1 Modules

The GENESSIS code is comprised of six (6) main modules (sub-routine packages) each with a single specific task. These are geometric; atmospheric, heat transfer, radiance, image, and ephemeris. With the exception of the ephemeris module, these packages are discussed in detail in Sections 2.2.1 through 2.2.5. The ephemeris module computes the altitude-azimuth position of the sun for any specific time, date and observer location. A published user's manual exists for this package.*

2.1.2 Module Interaction

A flow diagram of the GENESSIS architecture is given in Figure 2-1 which details module interaction and hierarchy. The geometric, ephemeris, atmospheric and image modules have independent capabilities. The radiance module is dependent upon the heat transfer module and requires inputs in real time.

*Solar Ephemeris Algorithm, W. Wilson. Visibility Laboratory, Scripps Institution of Oceanography, UCSD. S10 Ref. 80-13, July 1980, La Jolla, CA.

2.1.3 User Input/Control

User inputs are categorized according to purpose. These are geometric, sensor, atmospheric, and orbital. The elements of these are:

2.1.3.1 Geometric Inputs

- (a) The date and time of the simulation used to compute the position of the sun.
- (b) The latitude and longitude of the viewer subsatellite point.
- (c) The observer altitude in kilometers.

2.1.3.2 Sensor Inputs

- (a) The vertical and horizontal angular field-of-view.
- (b) Focal plane rotation in degrees.
- (c) The vertical and horizontal spatial resolution in meters.

2.1.3.3 Atmospheric Inputs

- (a) Atmospheric model (six LOWTRAN standard atmospheres).
- (b) Aerosol model.
- (c) Haze model.
- (d) Visibility in kilometers.

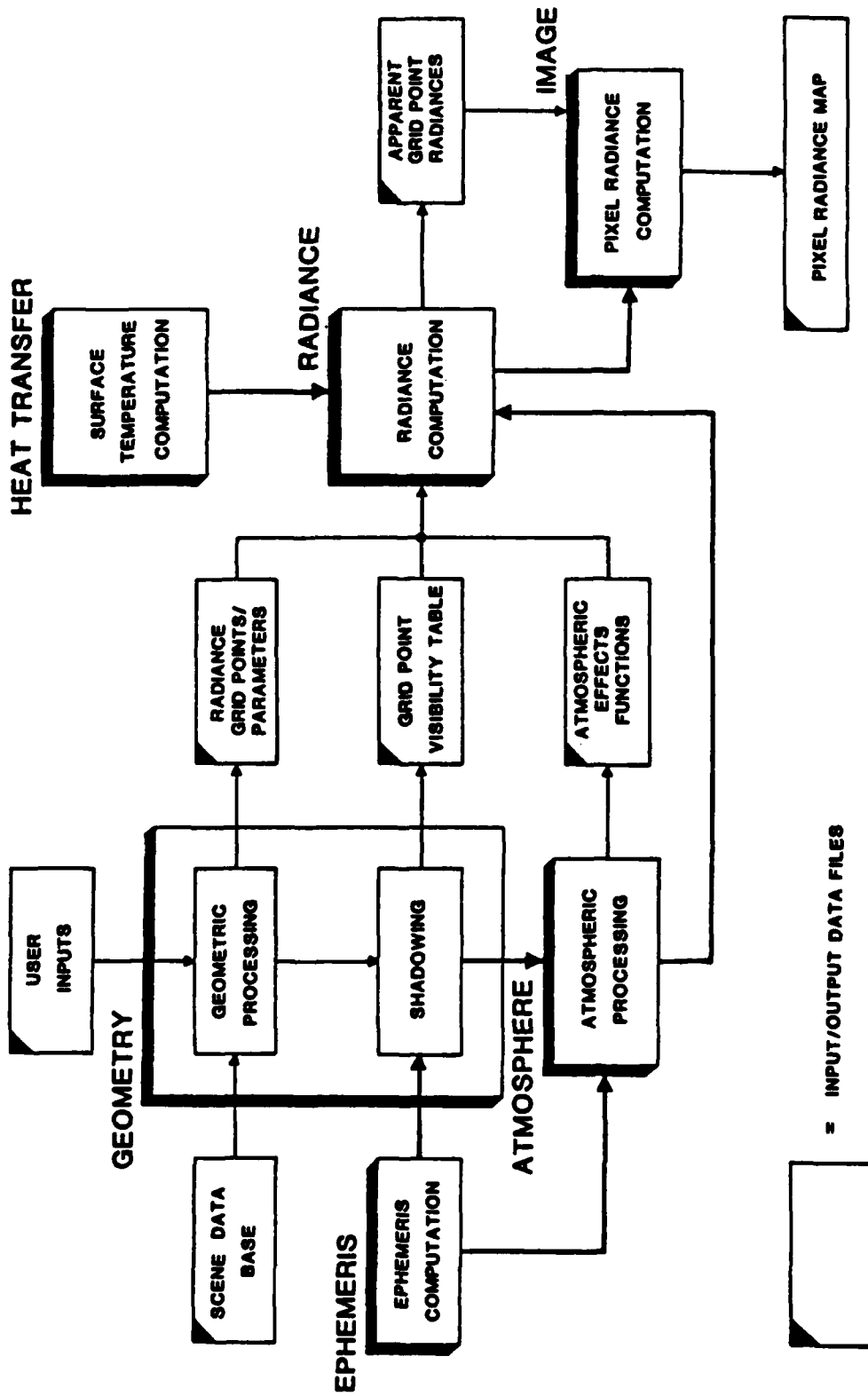


Figure 2-1. GENESIS Architecture

2.1.3.4 Orbital Inputs (Scene Sequencing Option)

- (a) Orbital inclination angle with respect to the equator.
- (b) Longitude of ascending node.
- (c) Framing rate.
- (d) Number of total frames.

2.1.4 Scene Data Base Inputs

Scene data inputs consist of the altitude, material type pairs which were mentioned previously, plus thermal, atmospheric, and reflectance data. The elements of these inputs are:

- (a) Material thermal properties (solar absorptance, thermal emittance, thermal conductance and thermal mass) required by the heat transfer module.
- (b) Material in-band diffuse reflectance.
- (c) Cloud in-band bi-directional reflectance.
- (d) Surface level atmospheric properties (temperature, wind speed, and humidity).

2.2 Module Description

2.2.1 Geometry

The geometric module supplies information regarding the visibility, orientation and projection of scene radiance grid points. All geometric calculations are based on an earth centered Cartesian coordinate system.

Surfaces and normal vectors are produced from the scene data using a bi-cubic spline fitting technique. In the event grid points are required at a higher resolution than the scene input data, they are generated from the spline-fit produced surfaces.

The visibility of each grid point is determined using a hidden line masking technique. The scene is processed twice, once for the observer and once for the sun. Points not visible to the observer are ignored. Points not seen by the sun are in shadow and are treated accordingly by the radiance module.

Projection of each point into the observer's image plane completes the primary task of the geometric module. The module is diagrammed in Figure 2-2.

2.2.2 Atmospheric Module

The atmospheric module supplies LOWTRAN-derived data for one of six standard atmospheres. It computes four in-band parameters: reflected solar, reflected skyshine, path transmission and path radiance. The reflected components are apparent values, having been attenuated spectrally along the observer's line-of-sight path. Path transmission and path radiance are computed for the path from the surface to the observer only. This path transmission attenuates the surface emission. For the reflected components, the atmospheric module calculates path transmission and radiance spectrally for the path from source to the surface and to the observer. The spectral data are then integrated over wavelength to produce a simple in-band value for the entire path.

In order to reduce the long-term costs associated with the computation of atmospheric parameters, and to provide the necessary computational flexibility, it is desirable to have the atmospheric parameters functionally related to altitude. Early investigations showed that these parameters could be represented by polynomials over the altitude range from 0 to 10 km.

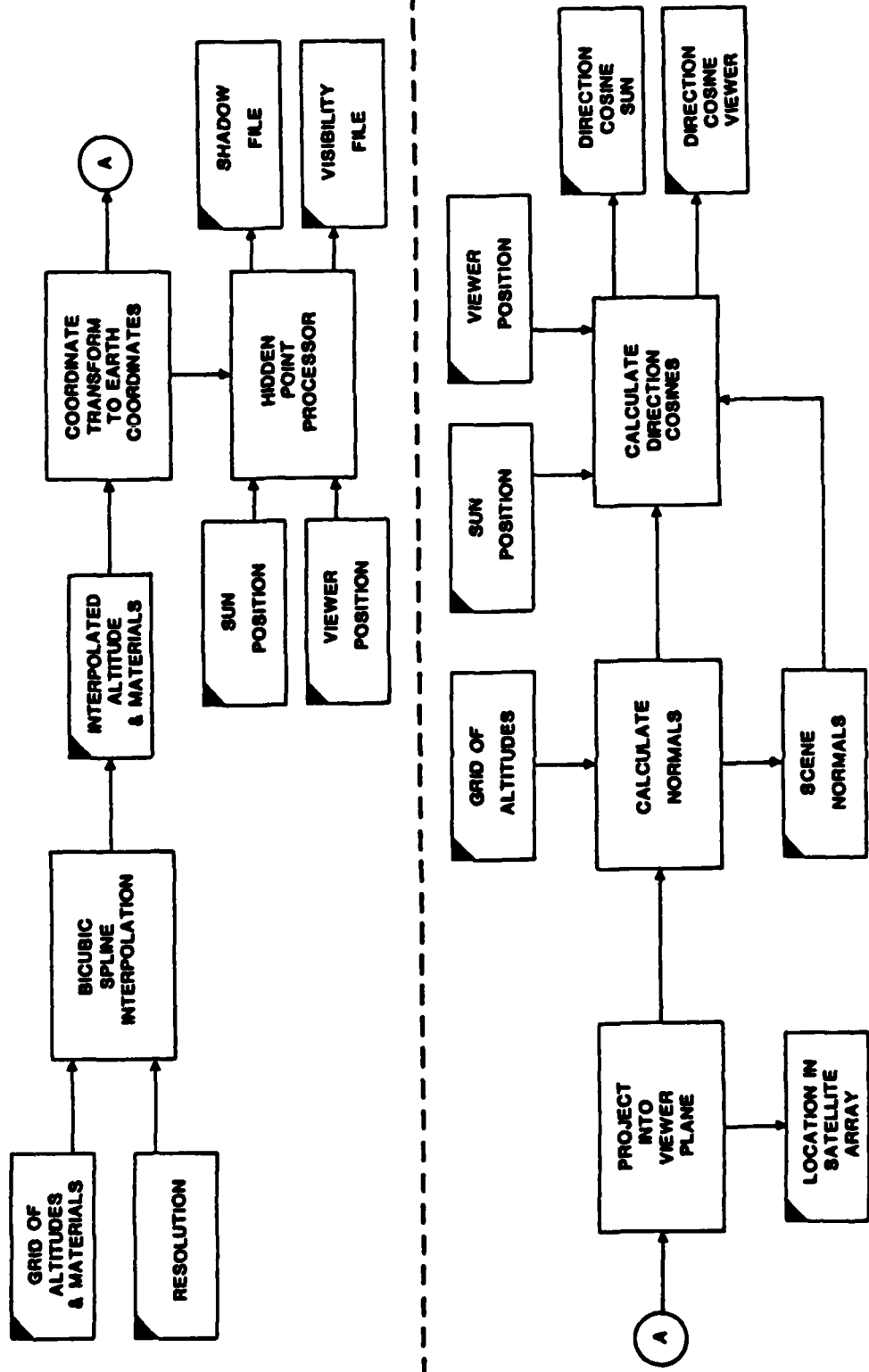


Figure 2-2. Geometric Module

Parameters are calculated parametrically for a series of zenith angles and altitudes. At each altitude a polynomial fit versus air mass is computed and stored for reflected solar, path transmission and path radiance. For skyshine, polynomial fits are stored as a function of altitude only. From this data base, polynomial fits versus altitude for each of the four atmospheric parameters are produced for any given solar and observer position.

Since the reflected solar component is also a function of the solar zenith angle, an additional series of cases and curve fits are required to completely describe this parameter.

Figure 2-3 is a flow diagram of the atmospheric module. Figures 2-4 through 2-7 illustrate sample atmospheric module outputs for the following conditions:

Atmosphere:	Subarctic Summer
Observer Altitude:	100km
Observer Zenith Angle:	0 degs
Sun Zenith Angle:	64 degs
Band:	7.5 - 12.0 μ m

2.2.3 Heat Transfer

Surface temperature is determined by the energy fluxes and thermal properties of the surface. The fluxes considered in the model are those resulting from solar irradiance, sky irradiance, convection to the air, self-emitted radiation, latent heat flux due to evaporation of surface moisture, and the distributed flux through the material to a substrate. The heat balance solution of the dynamic surface temperature employs two simplifying assumptions. These are that the lateral heat flux at the surface is zero, and that the distributed heat flux to the substrate can be calculated using n discrete layers, the lowest of

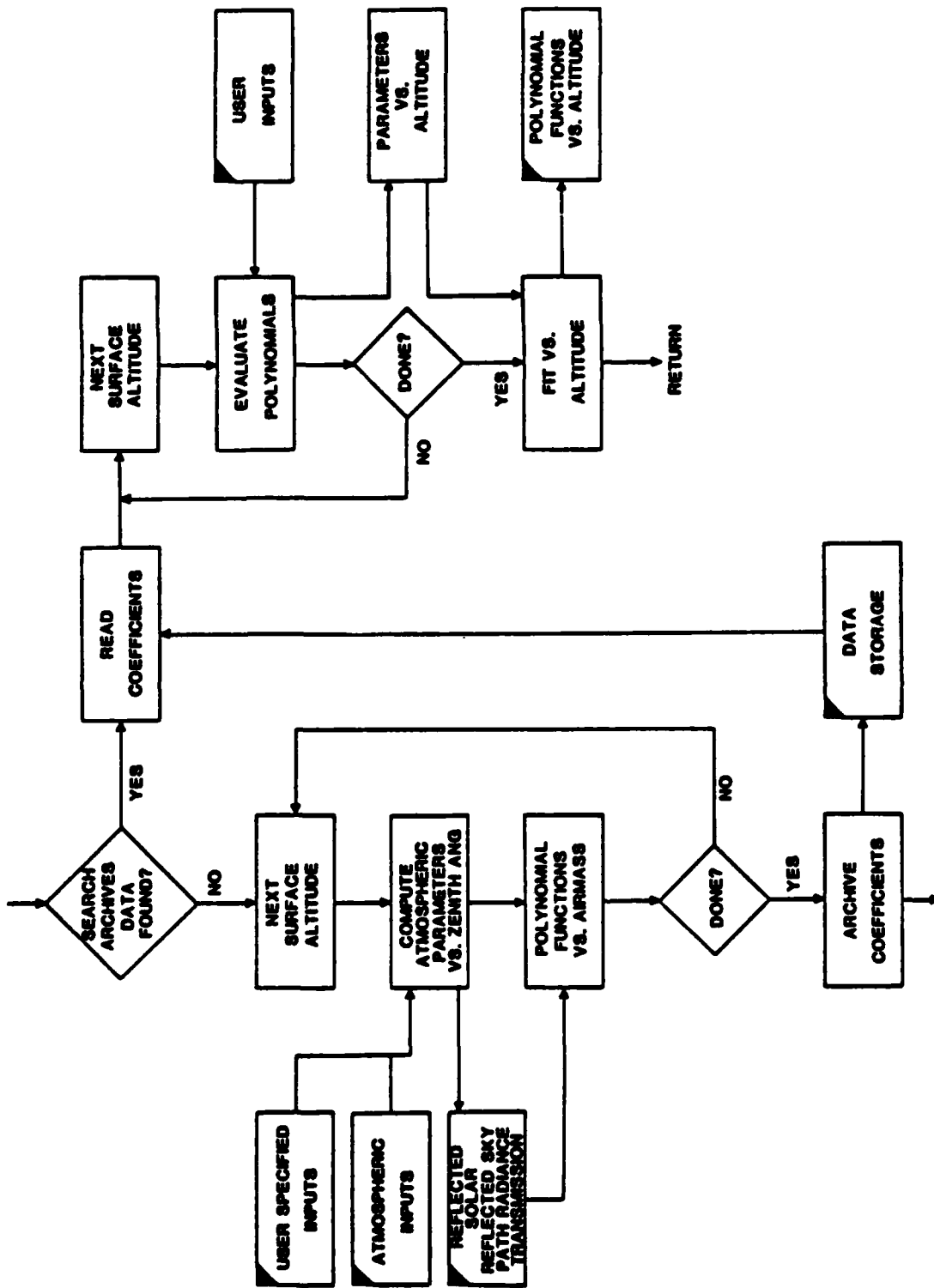


Figure 2-3. Atmospheric Module

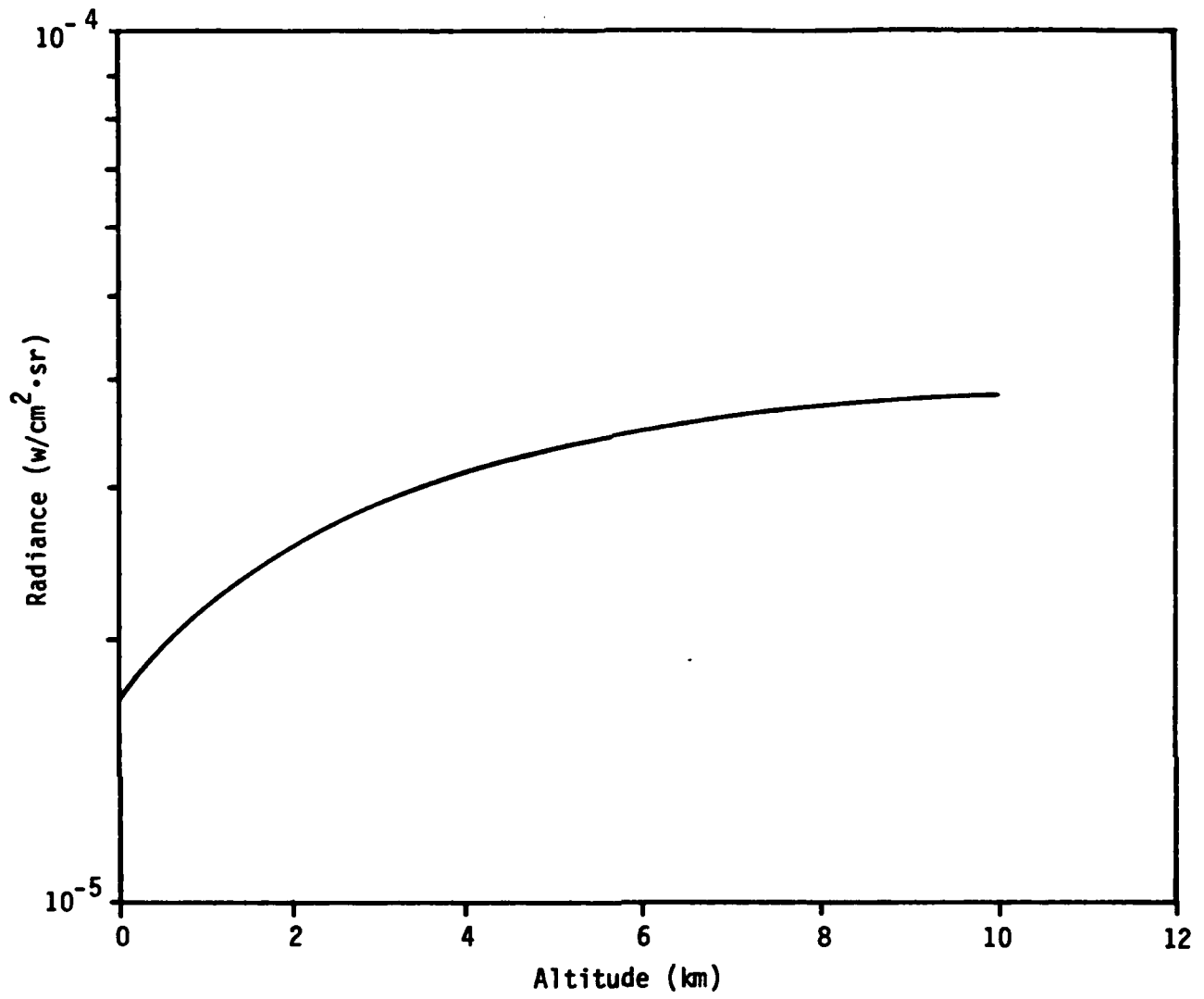


Figure 2-4. Apparent reflected solar radiance versus altitude

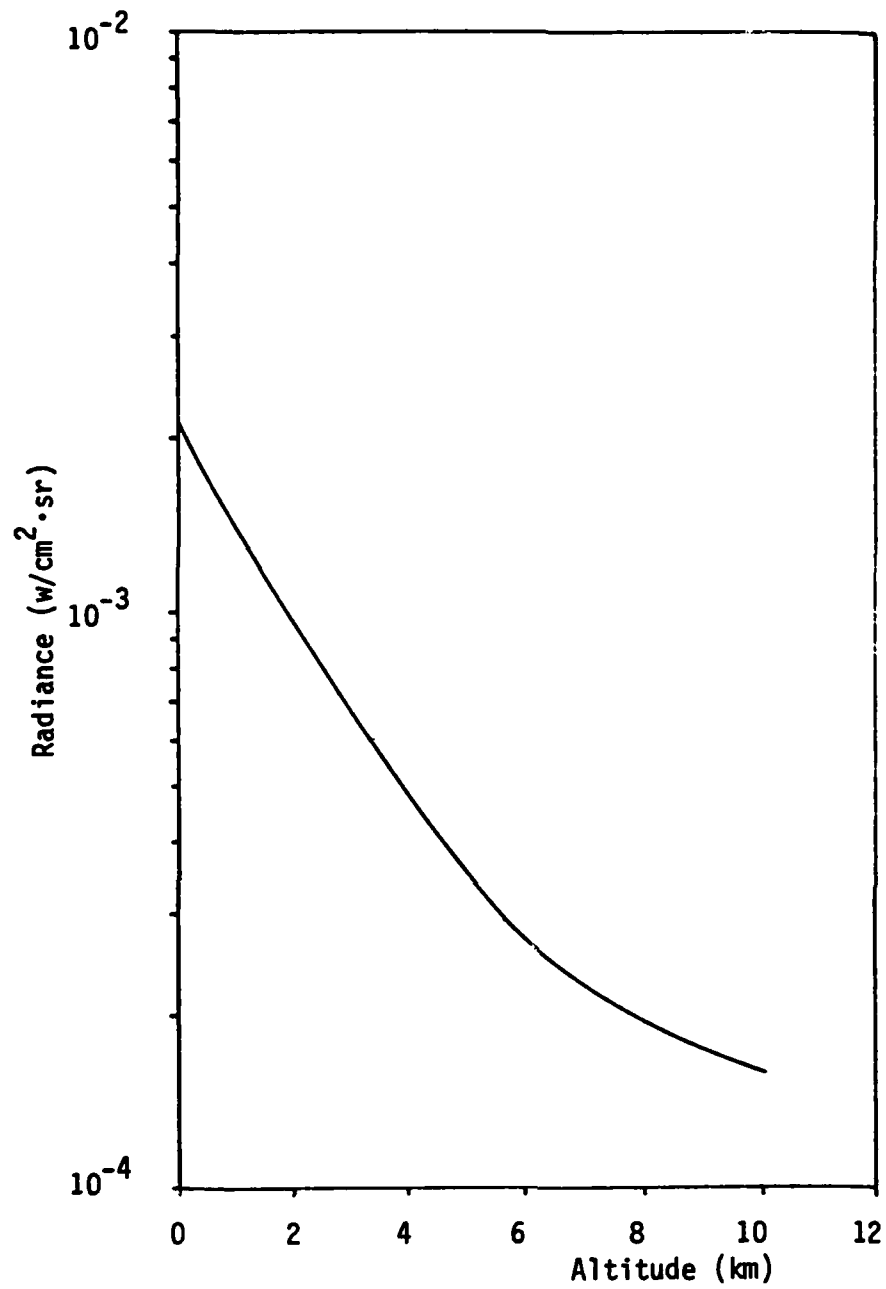


Figure 2-5. Skyshine apparent radiance versus altitude

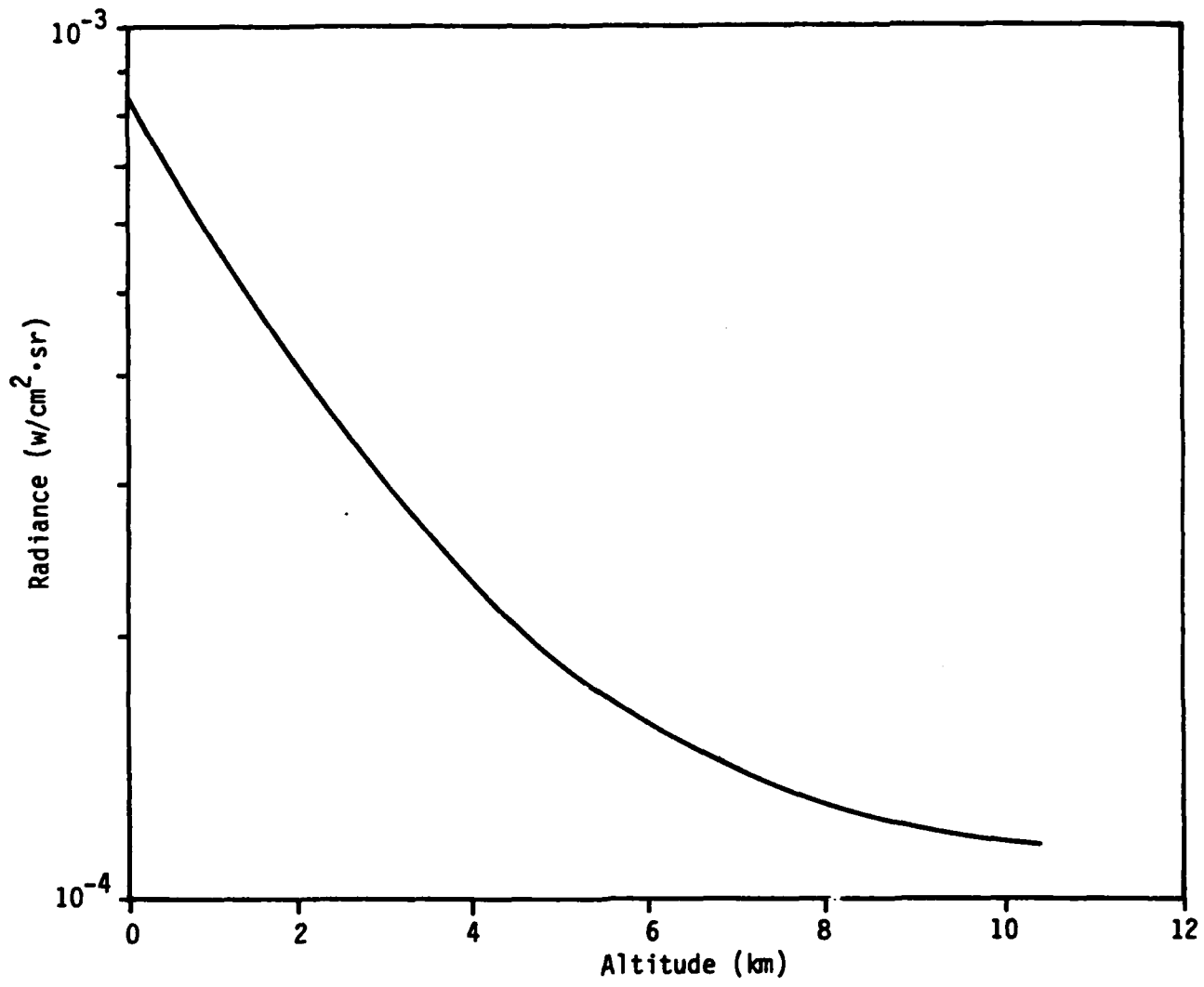


Figure 2-6. Path radiance versus altitude (km)

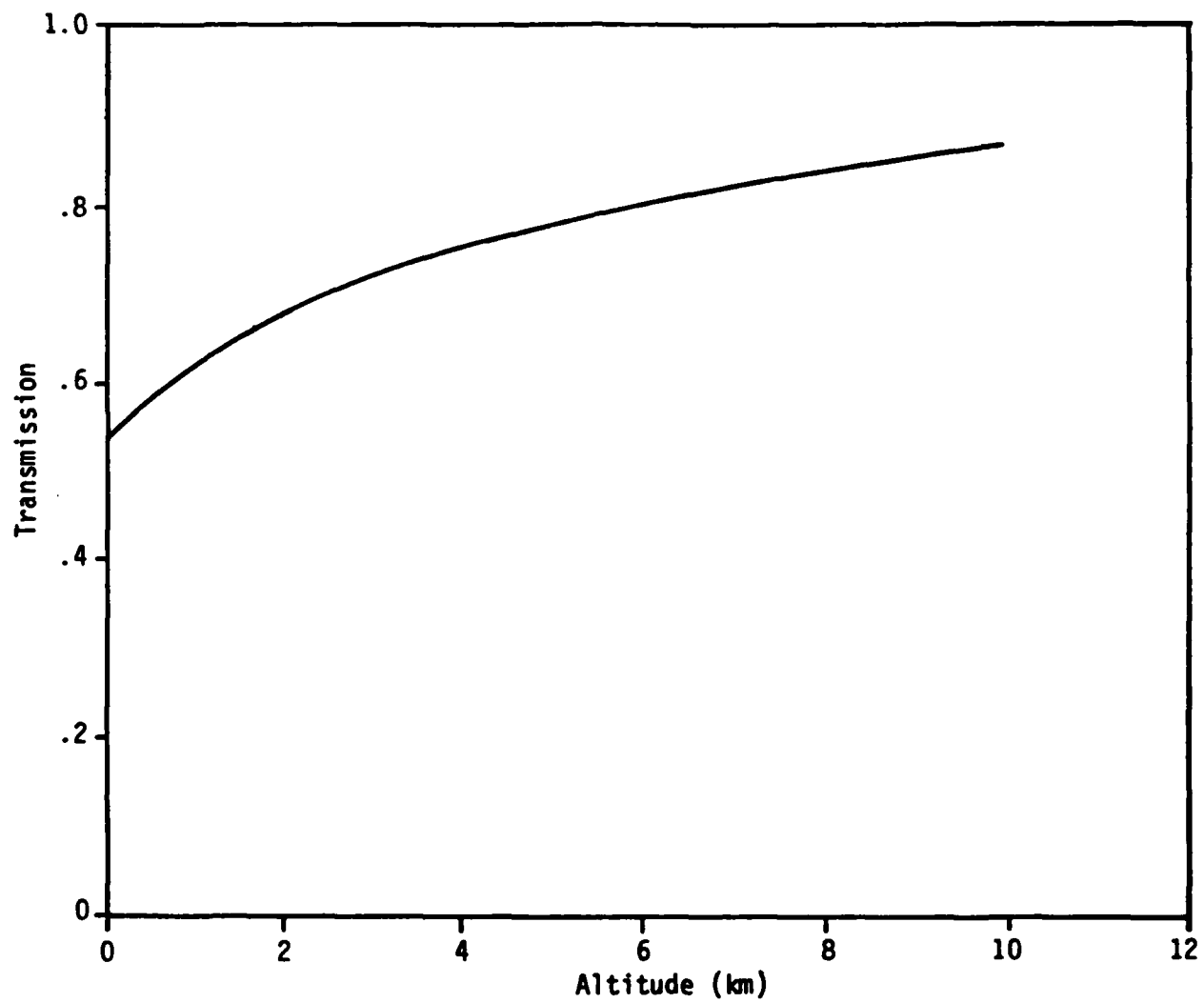


Figure 2-7. Path transmission versus altitude

which is adjacent to a diurnally constant subsurface. The result and physical model and its equivalent electrical circuit are given in Figure 2-8.

The heat balance equation for the physical model is

$$\phi_{\text{sun}} + \phi_{\text{sky}} + \phi_{\text{stored}} = \phi_{\text{conv}} + \phi_{\text{evap}} + \phi_{\text{emit}} + \phi_{\text{cond}} \quad (2-1)$$

All fluxes are in units of W/m^2 and all vary with time. Each of these fluxes is expressed as follows.

The solar irradiance flux, ϕ_{sun} , is calculated by

$$\phi_{\text{sun}} = \alpha(s)E(\text{sun},t)\cos\zeta(t) \quad (2-2)$$

where

$\alpha(s)$ is the effective solar absorptance,

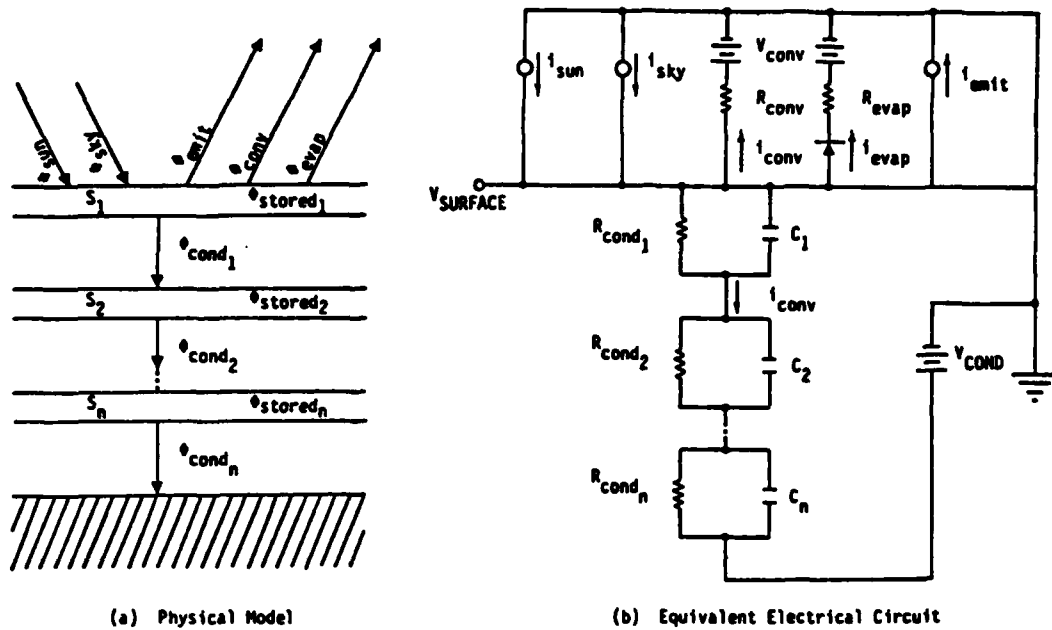
$\zeta(t)$ is the time dependent angle between the vector to the sun and the surface normal vector, and

$E(\text{sun},t)$ is the time dependent solar irradiance at the surface.

The solar irradiance at the surface is given by

$$E(\text{sun},t) = E_{\psi_0}(\text{sun},h) \cdot f(\psi)(t), \quad (2-3)$$

where $E_{\psi_0}(\text{sun},h)$ is the zenith solar irradiance as a function of surface altitude, h , and $f(\psi)$ is a factor to correct for increasing atmospheric attenuation with increasing solar zenith angle ψ .



(a) Physical Model

(b) Equivalent Electrical Circuit

FLUX DEFINITION

- | | | | |
|------------|--------------------|--------------|------------------------|
| i_{sun} | = solar irradiance | i_{evap} | = surface evaporation |
| i_{sky} | = sky irradiance | i_{stored} | = layer stored |
| i_{emit} | = emission | i_{conv} | = air convection |
| | | i_{cond} | = substrate conduction |

Figure 2-8. Surface temperature heat balance model

The sky irradiance flux, ϕ_{sky} , is computed from the Idso-Jackson formula

$$\phi_{sky} = \alpha(L)\sigma T_a^4 \{1 - 0.261 \exp[-7.77 \times 10^4 (273 - T_a)^2]\} \quad (2-4)$$

where

σ is the Stephan-Boltzmann constant, $5.6687 \times 10^{-8} \text{ W/m}^2 \cdot \text{K}$,

T_a is the ambient air temperature, and

$\alpha(L)$ is the effective thermal absorptance.

The convective flux to the atmosphere is computed by

$$\phi_{conv} = \rho c D W (T - T_a) \quad (2-5)$$

where

ρ is the ambient air density,

c is the specific heat of dry air,

D is the drag coefficient, empirically determined from ground truth data ranging from 0.002 to 0.01 depending upon the material,

W is the wind speed factor, equal to $1 + V_w$ where V_w is the wind speed in m/sec, and

T is the surface temperature.

The latent heat flux is computed by

$$\phi_{evap} = 0.622 \rho D W e (v - v_a) / \rho_a \quad (2-6)$$

where

- e is the latent heat of evaporation,
- v is the vapor pressure at the surface,
- v_a is the vapor pressure of the air, and
- p_a is the atmospheric pressure.

If v_a is larger than v, φ_{evap} is set equal to zero.

The emitted flux is computed by

$$\phi_{\text{emit}} = \epsilon(L) \sigma T^4 \quad (2-7)$$

where δ(L) is the effective thermal emittance, set equal to α(L) in Equation (2-4).

The conductance flux to the substrate is computed by

$$\phi_{\text{cond}} = g (T - T_s)$$

where g is the conductance to the substrate, equal to l_s·K where l_s is the depth at which the soil is diurnally constant and K is the soil conductivity, and T_s is the substrate temperature.

The stored flux in the surface layer is computed by

$$\phi_{\text{stored}} = l_o C [T(t+\Delta t) - T(t)] / \Delta t \quad (2-8)$$

where

- l_o is the layer thickness,
- C is the heat capacity of the surface material, and
- ΔT is the time increment.

The solution for the surface temperature T is achieved using an iterative method wherein the surface temperature is initially chosen as the ambient air temperature at midnight, and the heat balance equation is iteratively evaluated in time increments Δt (usually set equal to 30 minutes). This iteration is continued until successive diurnal cycles match, commonly occurring within three days.

This procedure is used to produce a data base for all materials within the scene. All independent variables are varied over a sufficient range so as to bracket all conditions that may be encountered in the scene. These independent variables are:

- (a) Peak solar irradiance,
- (b) Air-surface convective flux,
- (c) Air-surface evaporative flux,
- (d) Substrate-surface conductive flux,
- (e) Time.

The data base is compressed using a technique by which only the j most informative time points are retained of the i that were calculated. This results in a significant reduction in size of the data base (i usually 48, j/i usually 1/6) with little reduction in accuracy.

2.2.4 Radiance Module

The apparent radiance of a specific grid point is composed of four terms combined additively. These include reflected solar, thermal emission, reflected skyshine and path radiance.

2.2.4.1 Reflected Solar

The apparent reflected solar component is

$$N_{\text{solar}} = \rho \phi_{\text{solar}}(h) \cos \theta$$

where

- ρ = surface in-band diffuse reflectance (bi-directional reflectance for clouds),
- $\phi_{\text{solar}}(h)$ = computed fit to apparent reflected solar versus altitude (supplied by atmospheric module),
- h = surface altitude in km, and
- θ = local sun zenith angle (the angle between the vector to the sun and the surface normal).

2.2.4.2 Thermal Emission

The thermal emission component is given by

$$N_{\text{thermal}} = \epsilon \tau(H) \int_{\lambda_1}^{\lambda_2} N(\lambda, T_s) d\lambda$$

where

- ϵ = surface emissivity,
- ρ = surface in-band diffuse reflectance (1- ϵ),
- $\tau(h)$ = computed fit to path transmission versus altitude (supplied by the atmospheric module),
- h = surface altitude in km,
- λ_1, λ_2 = beginning and ending band wavelengths in μm ,
- $N(\lambda, T_s)$ = Planck function, and
- T_s = equilibrium surface temperature in Kelvin (supplied by the heat transfer module).

2.2.4.3 Reflected Skyshine

The apparent reflected skyshine component is given by

$$N_{\text{sky}} = \rho \phi_{\text{sky}}(h)$$

where

- ρ = surface in-band diffuse reflectance,
- $\phi_{\text{sky}}(h)$ = computed fit to apparent reflected skyshine versus altitude (supplied by the atmospheric module), and
- h = surface altitude in km.

2.2.4.4 Path Radiance

Path radiance is given by

$$N_{\text{path}} = \phi_{\text{path}}(h)$$

where

- $\phi_{\text{path}}(h)$ = computed fit to path radiance versus altitude (supplied by the atmospheric module), and
- h = surface altitude in km.

The total apparent surface radiance returned by the radiance module for a single grid point is

$$N_{\text{apparent}} = N_{\text{solar}} + N_{\text{thermal}} + N_{\text{sky}} + N_{\text{path}}$$

Two additional calculations are made by the radiance module. These are the total (overall wavelengths) solar and skyshine irradiances required by the heat transfer module.

The total surface solar irradiance was approximated utilizing LOWTRAN 5 path transmissions computed spectrally at 20 cm^{-1} resolution in the 0.25 to $4.0 \text{ }\mu\text{m}$ region (nearly 99% of the sun's total exoatmospheric irradiance is emitted between 0.25 and $4.0 \text{ }\mu\text{m}$) and a blackbody the size, distance and effective temperature of the sun. Exoatmospheric irradiance is attenuated spectrally and integrated over wavelength to yield the total surface solar irradiance.

Total diffuse sky irradiance is computed from a pressure compensated Idso-Jackson formulation.

Functional relations between solar and diffuse sky irradiance and altitude are computed off-line and are stored as data for each of the six standard atmospheres. The radiance module is diagrammed in Figure 2-9. Figures 2-10 and 2-11 illustrate the functional relation between solar and diffuse sky irradiances and altitude.

2.2.5 Imaging

A mean pixel radiance is computed for each pixel in the observer's image plane from the weighted sum of grid point apparent radiances projected into that pixel. That is,

$$\bar{N} = \frac{\sum_{i=1}^n W_i N_i}{\sum_{i=1}^n W_i}$$

where

- \bar{N} = mean apparent radiance of pixel,
- n = number of radiance points projected into pixel,
- W_i = weighting factor (equal $\cos \theta_i$),
- θ_i = angle between surface normal and vector to sun, and
- N_i = apparent radiance of grid point

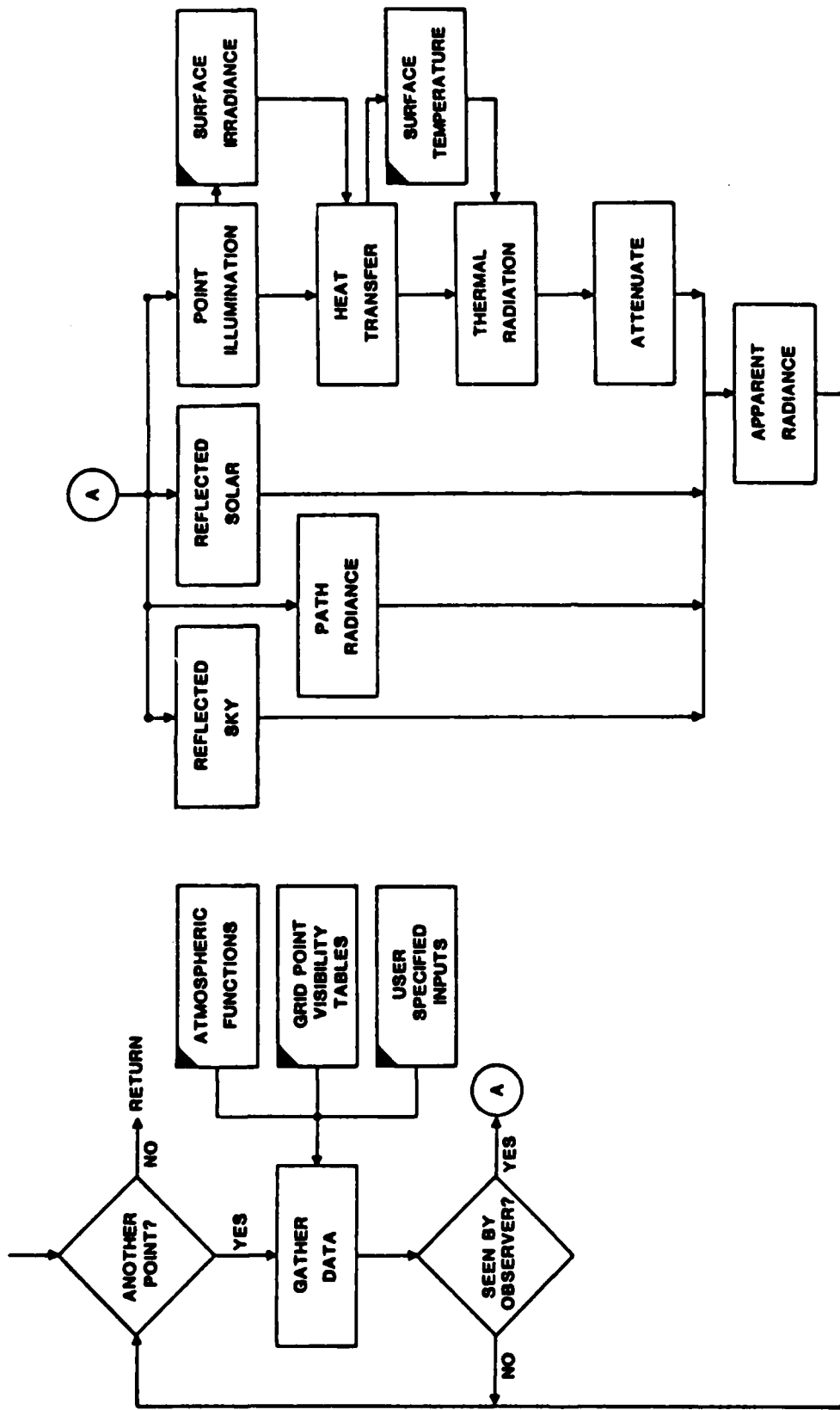


Figure 2-9. Radiance module

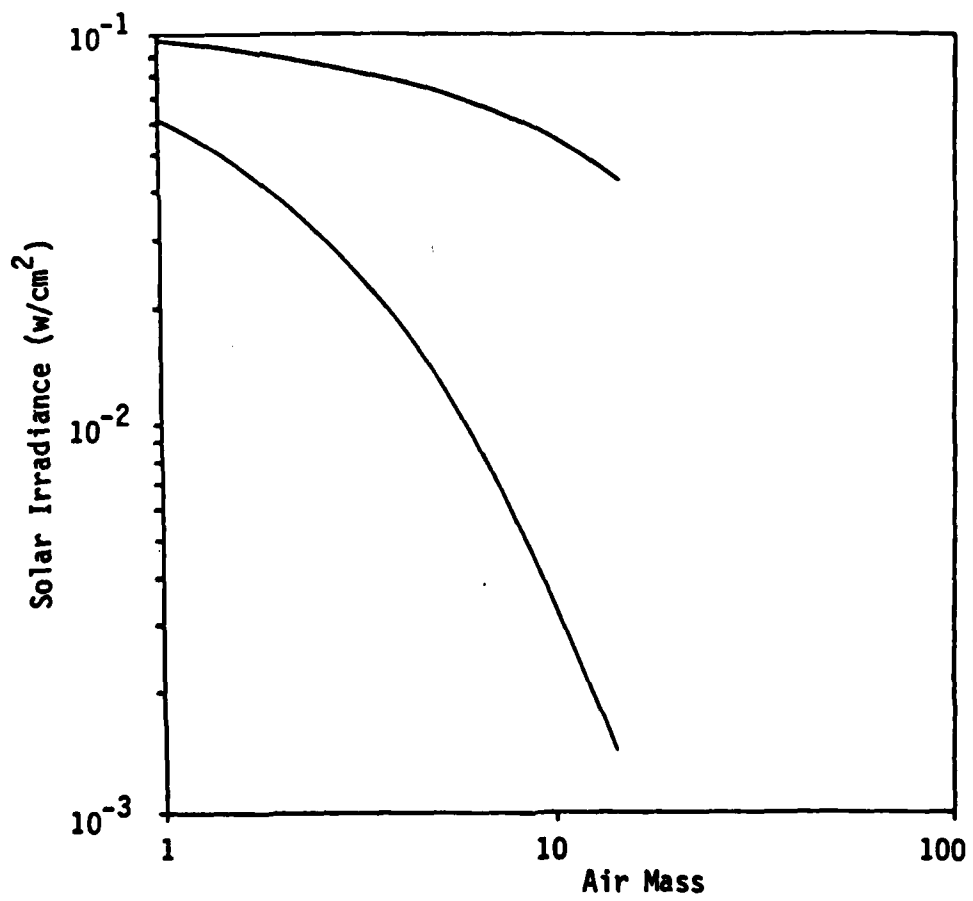


Figure 2-10. Solar irradiance versus air mass for standard atmosphere computes at 20 cm⁻¹ resolution

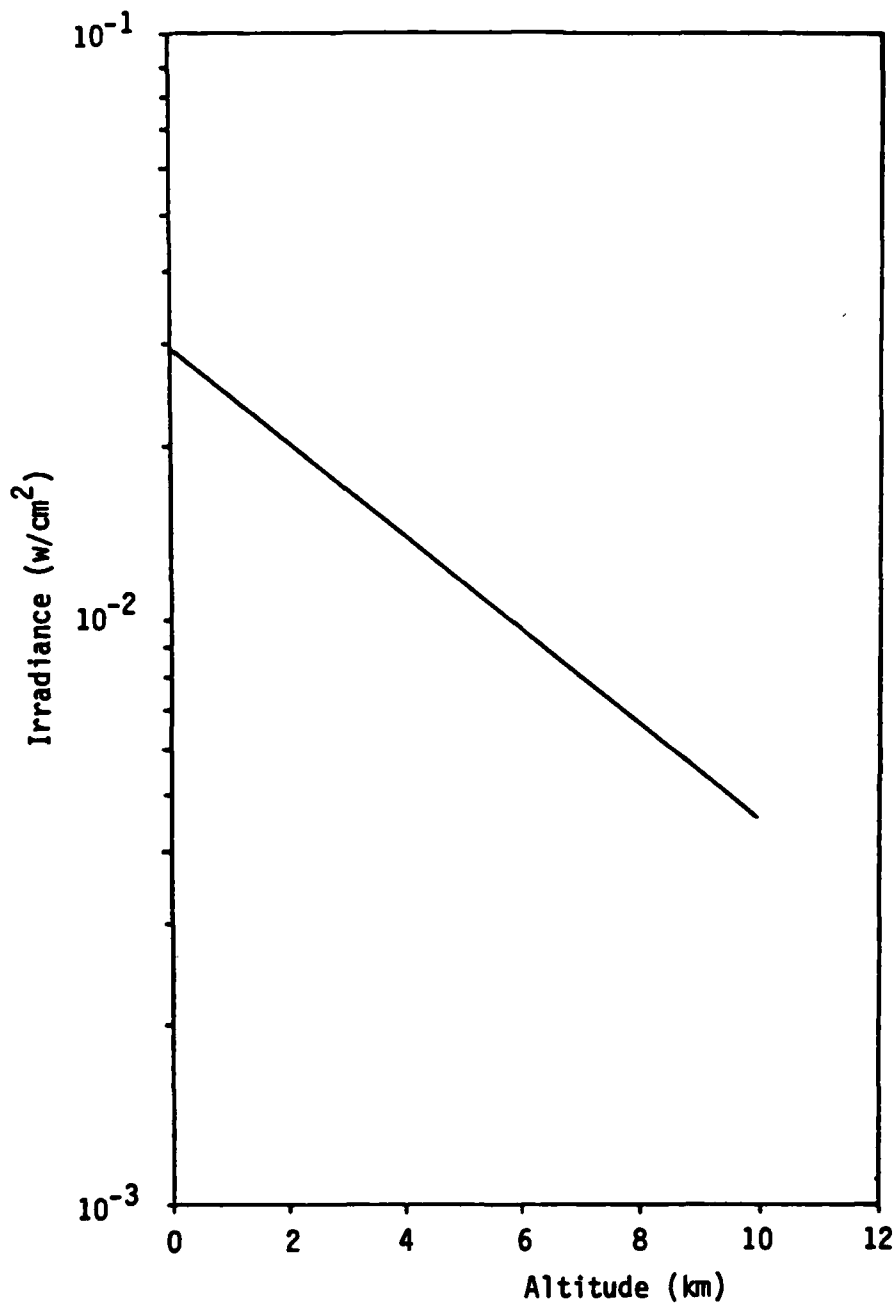


Figure 2-11. Idso-Jackson total diffuse sky radiance for U.S. standard atmosphere

The geometric module supplies both surface normal and projected grid point position in the observer's image plane. This produces an $N \times M$ viewer-perspective pixel apparent radiance map. The image module is diagrammed in Figure 2-12.

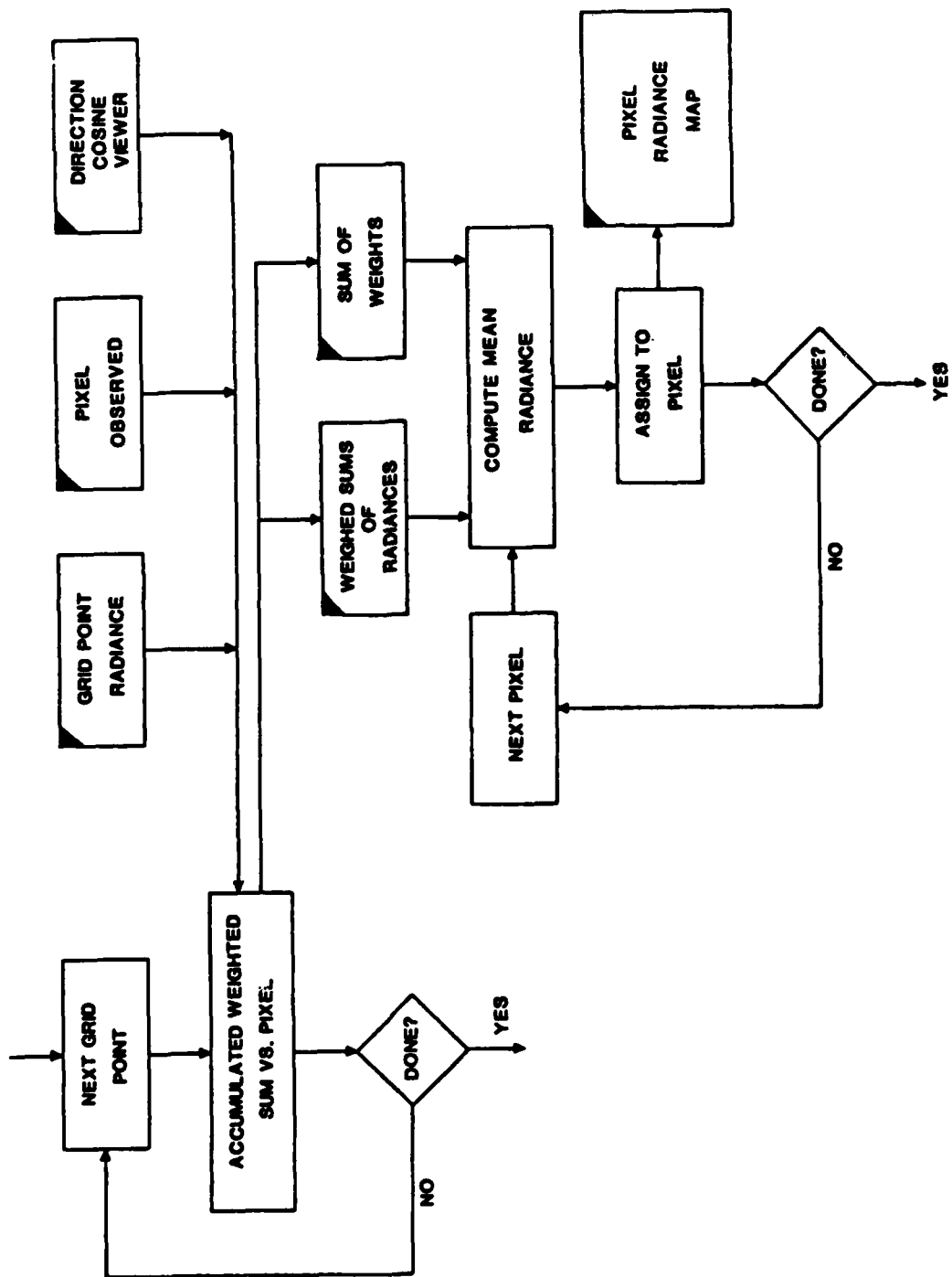
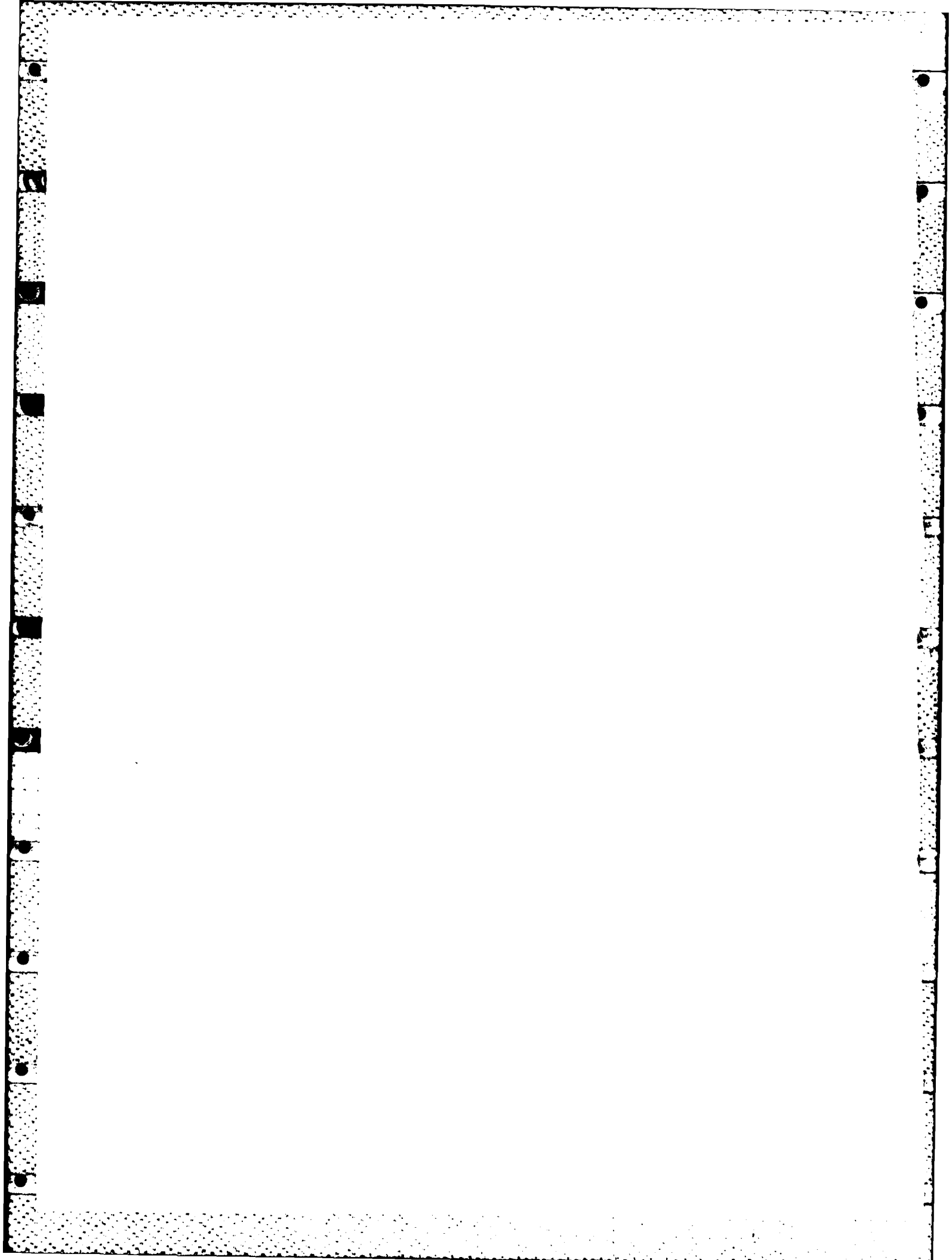


Figure 2-12. Image module



SECTION 3

HALO OPTICS

3.0 Introduction

The previous semiannual report described the three phase retrieval blind tests CSDL prepared for Eikonix. These tests were based on aberrations representing cryogenic deformations of an Itek HALO mirror 0.6m in diameter made of lightweight fused silica. The aberrations were scaled so that their peak-to-peak value was equal to one optical wavelength. The aberrated PSF was sampled by an 8 X 8 array of square detector elements, each element having a full width of $2.13 \lambda F$, where λ is the optical wavelength and F is the optical system focal ratio. To this array of signals, Gaussian random noise was added which had a uniform standard deviation of 2% of the peak diffraction-limited signal in the first two tests, and 5% in the third test. The second test also had a line-of-sight error of $(-0.984\lambda/D, -0.984\lambda/D)$, where D is the optical system pupil diameter. The data for the three tests is given in Table 3-1.

In this report a brief analysis of the aberrations is presented and the test results updated.

3.1 Aberration Analysis

The aberrations used in the phase retrieval tests were derived from the cryogenic deformations of an Itek HALO mirror. The aberration data is given in Table 3-2. The normalization factor is 100 so that

Table 3-1. Noisy and aberrated detector signals sent to Eikonix. The optical system has a circular pupil and the pixel width is $2.13\lambda F$. The origin (0,0) lies at the encircled number and the peak diffraction-limited signal is equal to 835. The noise is measured in terms of the peak diffraction-limited signal. (1) centered PSF and 2% noise. (2) PSF decentered by $(-0.984\lambda F, -0.984\lambda F)$ and 2% noise. (3) centered PSF and 5% noise.

CASE 1												
0	-10	-9	-5	-11	33	33	13	-7	-15			
7	6	1	27	33	30	4	4	-3	0			
6	-05	-16	2	29	179	12	12	27	0			
5	14	-2	6	66	352	50	50	-15	-4			
4	-2	12	1	61	95	50	50	-11	3			
3	29	-20	3	16	34	13	13	5	15			
2	-2	-6	26	35	11	-4	-4	-19	-14			
1	-16	-8	-12	-8	-15	-30	-30	-6	-25			
CASE 2												
0	26	-3	5	44	-13	-4	-4	27	-22			
7	-22	-33	4	21	11	5	5	-8	10			
6	2	13	-11	-29	56	14	14	6	9			
5	-10	3	10	102	249	29	29	13	1			
4	-15	-13	41	209	164	5	5	-8	21			
3	-2	11	16	-6	31	-2	-2	0	16			
2	-9	31	2	-12	20	-3	-3	16	-1			
1	-22	24	-8	-17	-21	-16	-16	-25	10			
CASE 3												
0	-34	-43	14	67	-16	-21	-21	51	100			
7	-30	41	22	-9	27	22	22	43	-7			
6	-5	53	-01	-32	166	-27	-27	24	-25			
5	53	-63	7	13	375	29	29	13	40			
4	87	-2	71	15	122	-2	-2	14	69			
3	16	21	-6	-68	56	-41	-41	16	-14			
2	8	-37	12	-2	-14	-94	-94	-91	-40			
1	34	-17	-88	45	-49	-41	-41	-23	-70			

Table 3-2. Aberrations used in the phase retrieval tests. The peak-to-peak value is 1λ , the normalization factor is 100.

-10	-9	-8	-7	-6	-5	-4	-3	-2	-1	0	1	2	3	4	5	6	7	8	9	10	
10	0	0	0	0	0	0	0	0	0	-12	0	0	0	0	0	0	0	0	0	0	
9	0	0	0	0	0	-30	-38	-26	-21	-19	-18	-16	-21	-23	0	0	0	0	0	0	
8	0	0	0	0	-34	-24	-31	-20	-13	-21	-15	-9	-15	-18	-22	-20	0	0	0	0	
7	0	0	0	-23	-24	-11	-14	-6	-5	-4	-3	-4	-10	-12	-17	-22	-19	0	0	0	
6	0	0	-20	-16	-9	-2	-6	-1	1	6	4	3	0	-4	-8	-12	-17	-21	-33	0	
5	0	0	-15	-9	1	1	3	4	14	16	13	11	6	2	-10	-21	-31	-39	0	0	
4	0	-10	-15	0	8	7	13	11	12	20	23	10	11	16	11	0	-11	-20	-28	-36	0
3	0	-10	-2	5	10	11	17	16	14	19	24	22	18	20	15	7	-1	-11	-18	-36	0
2	0	-7	4	10	11	13	22	23	17	16	20	26	28	23	16	14	5	-2	-10	-33	0
1	0	-7	6	10	14	20	30	27	19	17	18	20	28	23	17	22	12	1	-6	-30	0
0	-3	1	8	13	14	25	34	24	22	19	8	10	21	28	22	22	18	9	7	-12	-22
-1	0	3	5	14	14	23	31	30	23	18	4	8	16	25	24	21	16	13	6	-6	0
-2	0	-6	-1	12	13	14	22	30	23	15	11	8	13	21	21	16	12	10	-1	-10	0
-3	0	-2	1	11	10	11	13	20	17	12	12	15	16	18	18	17	14	12	3	-3	0
-4	0	-4	-1	4	3	3	9	8	12	11	10	10	9	17	16	16	15	19	13	2	0
-5	0	0	-11	-7	-2	1	1	3	4	4	4	5	5	10	9	10	15	18	20	0	0
-6	0	0	-22	-16	-14	-10	-6	-4	0	-1	-3	-2	1	3	7	9	13	12	15	0	0
-7	0	0	0	-29	-25	-27	-20	-15	-8	-13	-17	-21	-12	-8	0	3	2	1	0	0	0
-8	0	0	0	0	-33	-32	-36	-26	-16	-17	-35	-33	-28	-20	-18	-15	-13	0	0	0	0
-9	0	0	0	0	0	0	-50	-45	-37	-37	-87	-47	-37	-32	-31	0	0	0	0	0	0
-10	0	0	0	0	0	0	0	0	0	0	-65	0	0	0	0	0	0	0	0	0	0

the peak-to-peak aberration is 1λ . The array size is 21×21 corresponding to 317 rays inside a circular pupil. A plot of the aberrations is shown in Figure 3-1. The diffraction limited and aberrated point-spread functions are shown in Figures 3-2 and 3-3 respectively.

The aberrations were analyzed in terms of Zernike polynomials, given in Table 3-3. Starting with a standard deviation of 0.181λ and a Strehl ratio of 0.255, a 6-term (Z_4 through Z_8 , and Z_{11}) Zernike correction reduces the standard deviation to 0.081λ and increases the Strehl ratio to 0.7. An 8-term correction (Z_1 through Z_8), which now includes the two tilts (Z_2 and Z_3), does not change the image quality significantly indicating that the centroid of the spread function lies very close to the origin. A 15-term (Z_1 through Z_{15}) correction reduces the standard deviation to $\lambda/20$ and increases the Strehl ratio to 0.9. These results are summarized in Table 3-4.

3.2 Phase Retrieval Test Results

Eikonix estimated the aberrations from the noisy aberrated 8×8 array of point-spread function data in terms of Zernike polynomials. From the Zernike coefficients CSDL calculated the aberrations at a 21×21 array of points (within a circle) and subtracted them from the actual aberrations, thus making a correction. However, the residual aberrations were much worse than the initial ones. The standard deviation of the aberrations increased from an initial value of 0.186λ to approximately 0.4λ .

Various approaches such as the interchange of x and y coordinates, removal of the tilt aberrations, shift of the origin of the detector array coordinate system, addition instead of subtraction of aberrations, were tried to improve the system performance, but none worked. It was concluded that something had gone wrong with the Eikonix efforts.

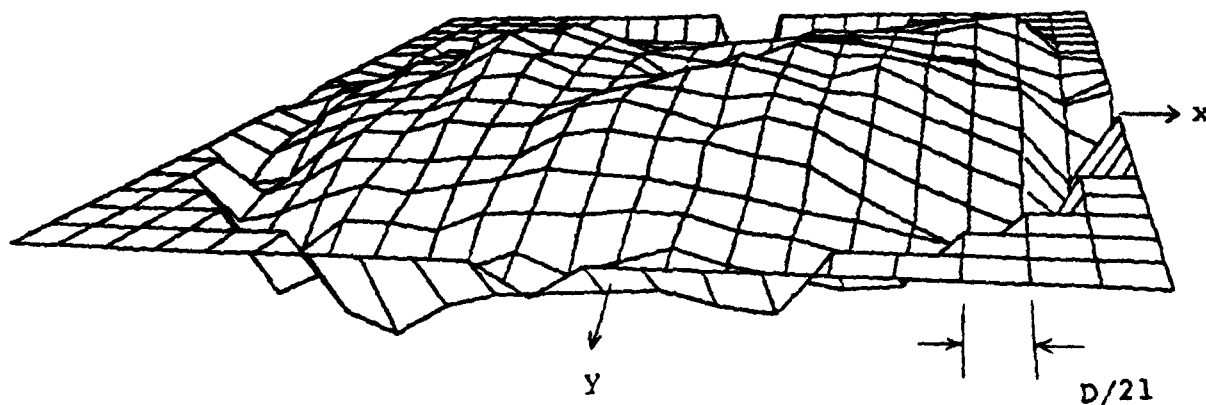


Figure 3-1. Plot of the aberration data

$$W_{p-p} = 1\lambda, \sigma_W = 0.186\lambda \quad D = \text{pupil diameter}$$

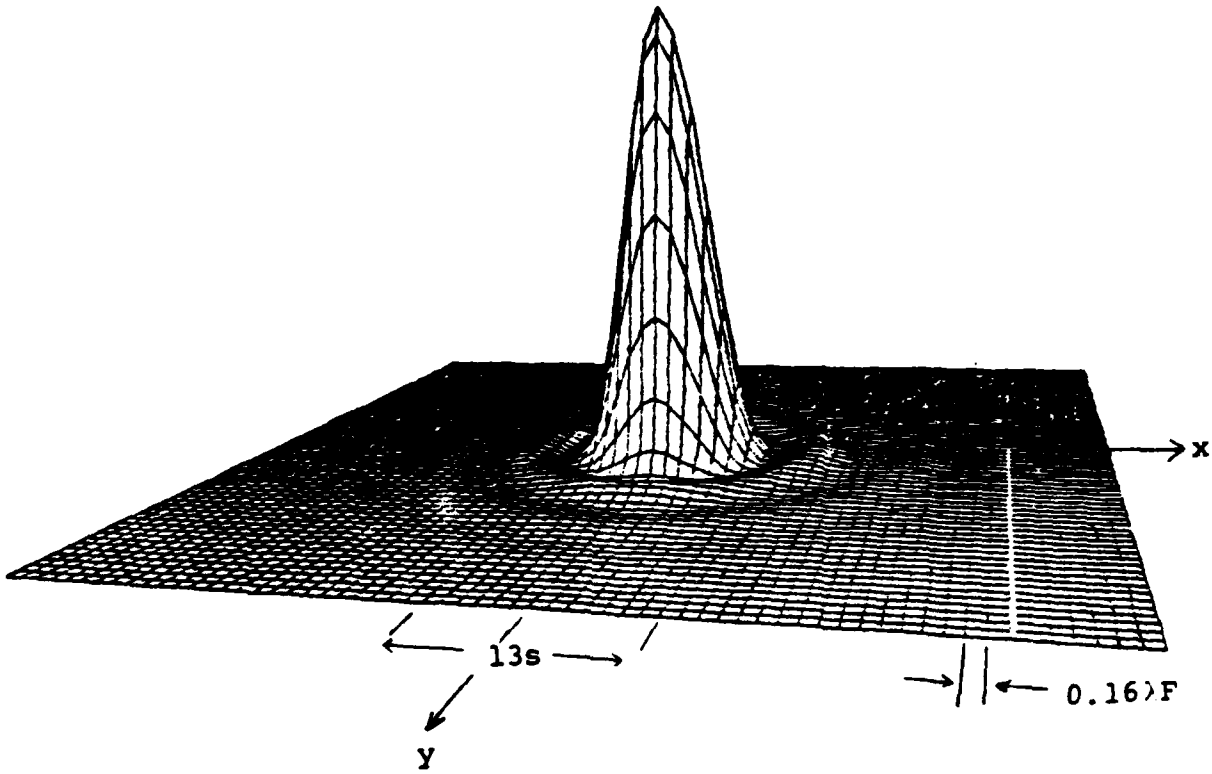


Figure 3-2. Diffraction limited point-spread function
 $s = 0.16\lambda F$. Detector width = $13s = 2.13\lambda F$.
 Airy disc diameter = $2.44\lambda F = 15s$.

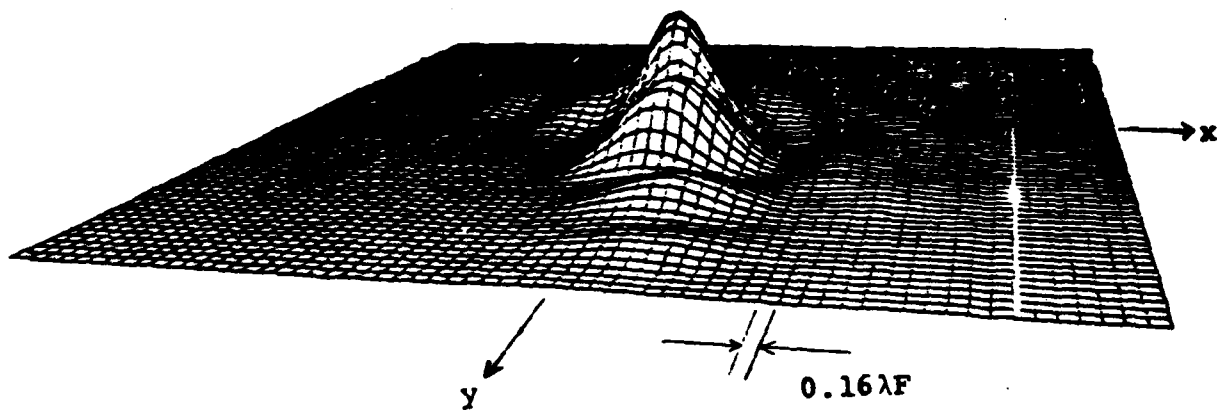


Figure 3-3. Aberrated point-spread function. PSF centroid lies at $(0.005\lambda F, 0.048\lambda F)$. The Strehl ratio is 0.255 and peak value is 0.277 at $(0, -0.32\lambda F)$.

Table 3-3. Zernike polynomials orthonormal over a unit circle. The modes, Z_j , are ordered such that even j corresponds to the symmetric modes defined by $\cos m\theta$, while odd j corresponds to the antisymmetric modes given by $\sin m\theta$. For a given n , modes with a lower value of m are ordered first.

Radial degree (n)	Azimuthal frequency (m)						
	0	1	2	3	4	5	6
0	$Z_0 = 1$ Constant						
1		$Z_1 = 2rcos\theta$ $Z_2 = 2rsin\theta$ Tilts (Lateral position)					
2	$Z_3 = \sqrt{3}(2r^2-1)$ Defocus (Longitudinal position)		$Z_4 = \sqrt{6}r^2sin2\theta$ $Z_5 = \sqrt{6}r^2cos2\theta$ Astigmatism (3rd order)				
3		$Z_6 = \sqrt{8}(3r^3-2r)sin\theta$ $Z_7 = \sqrt{8}(3r^3-2r)cos\theta$ Coma (3rd order)		$Z_8 = \sqrt{8}r^3sin3\theta$ $Z_9 = \sqrt{8}r^3cos3\theta$			
4	$Z_{10} = \sqrt{5}(6r^4-6r^2+1)$ 3rd order spherical		$Z_{12} = \sqrt{10}(4r^4-3r^2)cos2\theta$ $Z_{13} = \sqrt{10}(4r^4-3r^2)sin2\theta$		$Z_{14} = \sqrt{10}r^4cos4\theta$ $Z_{15} = \sqrt{10}r^4sin4\theta$		
5		$Z_{16} = \sqrt{12}(10r^5-12r^3+3r)cos\theta$ $Z_{17} = \sqrt{12}(10r^5-12r^3+3r)sin\theta$		$Z_{18} = \sqrt{12}(5r^5-4r^3)cos3\theta$ $Z_{19} = \sqrt{12}(5r^5-4r^3)sin3\theta$		$Z_{20} = \sqrt{12}r^5cos5\theta$ $Z_{21} = \sqrt{12}r^5sin5\theta$	
6	$Z_{22} = \sqrt{7}(20r^6-30r^4+12r^2-1)$ 5th order spherical		$Z_{23} = \sqrt{14}(15r^6-20r^4+6r^2)sin2\theta$ $Z_{24} = \sqrt{14}(15r^6-20r^4+6r^2)cos2\theta$		$Z_{25} = \sqrt{14}(6r^6-5r^4)sin4\theta$ $Z_{26} = \sqrt{14}(6r^6-5r^4)cos4\theta$		$Z_{27} = \sqrt{14}r^6sin6\theta$ $Z_{28} = \sqrt{14}r^6cos6\theta$

$$W(r,\theta) = \sum_{j=0}^{\infty} a_j Z_j(r,\theta) = \frac{1}{\pi} \int_0^{2\pi} \int_0^1 Z_j Z_j' r dr d\theta = \delta_{jj'}$$

Table 3-4. Analysis of aberrations used in the phase retrieval test in terms of zernike polynomials.

OPERATION	$\sigma_w(\lambda)$	STREHL RATIO
NO CORRECTION	0.181	0.255
6-TERM CORRECTION	0.081	0.7
8-TERM CORRECTION	0.081	0.7
15-TERM	0.05	0.9

Finally, under direction from RADC, CSDL gave Eikonix noise-free and aberration-free data sets, detailed procedures on how all the data had been generated and the actual aberrations to see if they could determine the source of their difficulty. They checked their software by duplicating our data. This time they obtained much more favorable results; the estimated aberrations looked quite similar to the actual ones. The residual aberrations had a standard deviation of 0.123λ giving a Strehl ratio of 0.556. However, they could not determine why the algorithm had not worked before. Of course, it was no longer a blind test.

CSDL suggested to RADC/DARPA that another blind test be carried out but this has not happened to date.

3.3 Image Sharpening Test Results

As reported earlier, CSDL's image sharpening algorithm, which works in a closed loop manner, was applied to the same noisy and aberrated spread-function data as the phase retrieval test. With six Zernike modal corrections (Z_4 through Z_8 and Z_{11}), the Strehl ratio of the spread-function increased from 0.255 to 0.616 in one iteration. Due to the noise in the spread-function data, a second iteration did not improve the performance significantly.

3.4 Summary, Conclusions, and Recommendations

Eikonix's phase retrieval algorithms did not succeed on the blind test prepared by CSDL. The algorithm did work once all the information was disclosed to Eikonix. Unfortunately, Eikonix has not been able to determine why the algorithms failed on the blind test. These algorithms presumably work when (1) the peak-to-aberration is less than 1λ , (2) the pixel width is less than $2\lambda F$, and (3) the noise is less than 2%.

It would have been desirable to go through another blind test. It may still be desirable to do so. However, a hardware simulation should be prepared to test the practical limits of the applicability of the Eikonix algorithms.

CSDL's image sharpening algorithm has been demonstrated in both software and hardware simulations. It worked successfully on the same noisy and aberrated spread-function as the Eikonix phase retrieval algorithm. It appears to be a robust and powerful technique for adaptive correction of aberrated images. It can be used both in closed-loop image correction mode or phase retrieval mode.

addresses	number of copies
R. Carman RADC/OCSE	5
RADC/TSLD GRIFFISS AFB NY 13441	1
RADC/DAP GRIFFISS AFB NY 13441	2
ADMINISTRATOR DEF TECH INF CTR ATTN: DTIC-DDA CAMERON STA BG 5 ALEXANDRIA VA 22314	12
Charles Stark Draper Laboratory, Inc 555 Technology Square Cambridge, MA 02139	5
Charles Stark Draper Lab Attn: Dr. Keto Soosar 555 Technology Square M. S. -95 Cambridge, MA 02139	1
Charles Stark Draper Lab Dr. J. G. Lin 555 Technology Square Cambridge, MA 02139	1
Charles Stark Draper Lab Attn: Mr. R. Strunce 555 Technology Square M. S. -60 Cambridge, MA 02139	1

Charles Stark Draper Lab 1
Attn: Dr. Daniel R. Hegg
555 Technology Square
M. S. -60
Cambridge, MA 02139

ARPA/MIS 1
1400 Wilson Blvd
Arlington, VA 22209

ARPA/STO 1
Attn: Lt Col A. Herzberg
1400 Wilson Blvd
Arlington, VA 22209

ARPA/STO 1
Attn: Maj E. Dietz
1400 Wilson Blvd
Arlington, VA 22209

Riverside Research Institute 3
Attn. Dr. R. Kappesser
Attn. Mr. A. DeVilliers
1701 N. Ft. Myer Drive Suite 711
Arlington, VA 22209

Riverside Research 1
Attn: HALO Library, Mr. Bob Passut
1701 N. Ft. Myer Drive
Arlington, VA 22209

Itek Corp 1
Optical Systems Division
10 Maguire Rd.
Lexington, MA 02173

Perkin Elmer Corp 1
Attn: Mr. H. Levenstein
Electro Optical Division
Main Avenue
Norwalk, CT 06856

Hughes Aircraft Company 1
Attn: Mr. George Speak
M.S. B_156
Culver City, CA 09230

Hughes Aircraft Company 1
Attn: Mr. Ken Beale
Centinela Teale Sts
Culver City, CA 90230

Air Force Flight Dynamics Lab 1
Attn: Dr. Lynn Rogers
Wright Patterson AFB, OH 45433

AFWL/FIBG 1
Attn: Mr. Jerome Pearson
Wright Patterson AFB, OH 45433

Air Force Wright Aero Lab. FIEE 1
Attn: Capt Paul Wren
Wright Patterson AFB, OH 45433

Air Force Institute of Technology 1
Attn: Prof. R. Calico/ENY
Wright Patterson AFB, OH 45433

Aerospace Corp. 2
Attn: Dr. G. T. Tseng
2350 E. El Segundo Blvd
El Segundo, CA 90245

Aerospace Corp. 1
Attn: Mr. J. Mosich
2350 E. El Segundo Blvd
El Segundo, CA 90245

Aerospace Corp/Bldg 125/1054 1
Attn: Mr. Steve Burrin
Advanced Systems Tech Div.
2400 E El Segundo Blvd
El Segundo, CA 90245

SD/SD/YLVS 1
Attn: Mr. Lawrence Weeks
P. O. Box 92960
Worldway Postal Center
Los Angeles CA 90009

SD/YCD 1
Attn: YCPT/Capt Gajewski
P. O. Box 92960
Worldway Postal Center
Los Angeles, CA 90009

Grumman Aerospace Corp 1
Attn: Dr. A. Mendelson
South Oyster Bay Road
Bethpage, NY 11714

OUSDR&E/DS 1
Attn. Mr. A. Bertapelli
Room 3D136
Pentagon, Washington, DC 20301

Jet Propulsion Laboratory 2
Attn: Mr. D. B. Schaechter
4800 Oak Grove Drive
Pasadena, CA 91103

MIT/Lincoln Laboratory 1
Attn: S. Wright
P. O. Box 73
Lexington, MA 02173

MIT/Lincoln Laboratory 11
Attn: Dr. D. Hyland
P. O. Box 73
Lexington, MA 02173

MIT/Lincoln Laboratory Attn: Dr. N. Smith P. O. Box 73 Lexington, MA 02173	11
Control Dynamics Co. Attn: Dr. Sherman Seltzer Suite 1414 Executive Plaza 555 Sparkman Drive Huntsville, AL 35805	1
Lockheed Space Missile Corp. Attn: A. A. Woods, Jr., O/62-E6 p. O. Box 504 Sunnyvale, California 94088-3504	5
Lockheed Missiles Space Co. Attn: Mr. Paul Williamson 3251 Hanover St. Palo Alto, CA 94304	1
General Dynamics Attn: Ray Halstenberg Convair Division 5001 Keary Villa Rd San Diego, CA 92123	1
STI Attn: Mr. R. C. Stroud 20065 Stevens Creek Blvd. Cupertino, CA 95014	1
NASA Langley Research Ctr Dr. Earle K. Huckins III Attn: Dr. Card Langley Station Bldg 1293B M/s 230 Hampton, VA 23665	2
NASA Johnson Space Center Attn: Robert Piland Ms. EA Houston, TX 77058	1

<p>McDonald Douglas Corp Attn: Mr. Read Johnson Douglas Missile Space Systems Div 5301 Balsa Ave Huntington Beach, CA 92607</p>	1
<p>Integrated Systems Inc. Attn: Dr. N. K. Gupta and M. G. Lyons 151 University Avenue, Suite 400 Palo Alto, California 94301</p>	2
<p>Boeing Aerospace Company Attn: Mr. Leo Cline P. O. Box 3999 Seattle, WA 98124 MS B W-23</p>	1
<p>TRW Defense Space Sys Group Inc. Attn: Ralph Iwens Bldg 82/2054 One Space Park Redondo Beach, CA 90278</p>	1
<p>TRW Attn: Mr. Len Pincus Bldg R-5, Room 2031 Redond Beach, CA 90278</p>	1
<p>Department of the navy Attn: Dr. K. T. Alfriend Naval Research Laboratory Code 7920 Washington, DC 20375</p>	1
<p>Airesearch Manuf. Co. of Calif. Attn: Mr. Oscar Buchmann 2525 West 190th St. Torrance, CA 90509</p>	1
<p>Analytic Decisions, Inc. Attn: Mr. Gary Glaser 1401 Wilson Blv. Arlington, VA 22209</p>	1

Ford Aerospace & Communications Corp. 1
Drs. I. P. Leliakov and P. Barba, MS/GB0
3939 Fabian way
Palo Alto, California 94304

Center for Analysis 1
Attn: Mr. Jim Justice
13 Corporate Plaza
Newport Beach, CA 92660

General Research Corp. 1
Attn: Mr. G. R. Curry
P.O. Box 3587
Santa Barbara, CA 93105

General Research Corp 1
Attn: Mr. Thomas Zakrzewski
7655 Old Springhouse Road
McLean, VA 22101

Institute of Defense Analysis 1
Attn: Dr. Hans Wolfhard
400 Army Navy Drive
Arlington, VA 22202

Karman Sciences Corp. 1
Attn: Dr. Walter E. Ware
1500 Garden of the Gods Road
P.O. Box 7463
Colorado Springs, CO 80933

MRJ, Inc. 1
10400 Eaton Place
Suite 300
Fairfax, VA 22030

Photon Research Associates 1
Attn: mr. Jim Myer
P.O. Box 1318
La Jolla, CA 92038

Rockwell International 1
Attn: Russell Loftman (Space Systems Group)
(Mail Code - SL56)
12214 Lakewood Blvd.
Downey, CA 90241

Science Applications, Inc. 1
Attn: Mr. Richard Ryan
3 Preston Court
Bedford, MA 01730

U S. Army Missile Command 1
Attn: DRSMI-RAS/Mr. Fred Haak
Redstone Arsenal, AL

Naval Electronic Systems Command 1
Attn: Mr. Charles Good
PME_106-4
National Center I
Washington, DC 20360

Lockheed Palo Alto Research Laboratory 2
Attn: Dr. J. N. Aubrun, 0/52-56
3251 Hanover Street
Palo Alto, California 94304-1187

U. S. Army/DARCOM 1
Attn: Mr. Bernie Chasnov
AMC Bldg
5001 Eisenhower Ave
Alexandria, VA 22333

Defense Documentation Center 1
Cameron Station
Alexandria, VA 22314

Honeywell Inc. 2
Attn: Dr. Thomas B. Cunningham
Attn: Dr. Michael F. Barrett
2600 Ridgway Parkway MN 17-2375
Minneapolis, MN 55413

NASA Marshal Space Flight Center
Attn. Dr. J. C. Blair, ED01
Henry B. Waites
Marshal Space Flight Center, AL 35812

2

TRW
Attn: Robert Benhabib
Bldg 82/2024
One Space Park
Redondo Beach, CA 90278

1



MISSION
of
Rome Air Development Center

RADC plans and executes research, development, test and selected acquisition programs in support of Command, Control Communications and Intelligence (C³I) activities. Technical and engineering support within areas of technical competence is provided to ESD Program Offices (POs) and other ESD elements. The principal technical mission areas are communications, electromagnetic guidance and control, surveillance of ground and aerospace objects, intelligence data collection and handling, information system technology, ionospheric propagation, solid state sciences, microwave physics and electronic reliability, maintainability and compatibility.